Available online at www.sciencedirect.com
ScienceDirect
Nuclear Instruments and Methods in Physics Research B 259 (2007) 853–860
NIM B
Beam Interactions with Materials & Atoms
www.elsevier.com/locate/nimb

Comparative study of cascade damage in Fe simulated with recent potentials

C. Björkas *, K. Nordlund

Accelerator Laboratory, University of Helsinki, P.O. Box 43, FI-00014 Helsinki, Finland

Received 19 January 2007; received in revised form 19 March 2007
Available online 3 April 2007

Abstract

Considerable quantitative uncertainty has remained regarding the amount and structure of defects produced in molecular dynamics simulations of collision cascades in Fe. The problem is most likely related to the description of interstitial energetics in the interatomic potentials. Three potentials have recently been developed for Fe, which, even though they have different physical motivations and functional forms, describe the interstitial energetics well. Using these potentials, we simulate recoil collision cascades in Fe in the recoil energy range 0.5–20 keV. Prior to the cascade simulations a realistic high-energy repulsive part was added to two of the potentials, adjusting the fit to reproduce the experimentally obtained threshold displacement energies. The results show that the total Frenkel pair production, as predicted by the three potentials, is the same within the statistical uncertainty, but also that some differences remain in the fraction of clustered defects. However, these differences are smaller than those predicted by previous potentials.

PACS: 61.72.Ji; 61.80.Hg; 28.52.Fa; 34.20.Cf

Keywords: Fe; Molecular dynamics simulations; Displacement cascades; Interatomic potentials

1. Introduction

A first step in being able to understand neutron irradiation damage buildup in fission and fusion reactor steels, is knowing what the initial damage state produced by neutron-induced atomic recoils in Fe is. Supporting this is our recent study revealing that the primary damage in $Fe_{0.9}Cr_{0.1}$ is essentially the same as in pure Fe [1]. To be specific, we found that the chromium content did not affect the total number of defects nor the vacancy and interstitial clustered fractions. The primary state of the radiation damage in Fe in the heat spike regime has been extensively studied with computer simulations (for a recent overview see [2]), resulting in good qualitative understanding of the collision cascade development [3–5]. However, quantitative differences of more than a factor of three have remained in the predicted clustered defect production numbers [2,5], which can be a serious problem for modeling the longer time scale development of the defect evolution. Moreover, the disagreements between the potentials pose problems in finding a reliable predictive model for the behavior of Fe under irradiation. On the other hand, it is now well known that many of the interatomic potentials used have serious deficiencies in their description of e.g. the interstitial energetics, which is a likely cause to the differences [2].

In the current paper, we utilize three recent interatomic potentials for Fe which are comparable in overall quality and in particular reproduce the energetics of interstitials in different configurations in the correct order. These are the potential by Ackland, Mendelev and Srolovitz et al. (AMS) [6], the 'magnetic' potential by Dudarev and Derlet (DD) [7] and the Tersoff-like [8] analytical potential by Müller, Erhart and Albe (MEA) [9]. These potentials have very different physical motivations and functional forms. The AMS is a many-body potential of Finnis–Sinclair

* Corresponding author. Tel.: +358 9 19150003; fax: +358 9 19150042.
E-mail address: bjorkas@acclab.helsinki.fi (C. Björkas).

0168-583X/$ - see front matter © 2007 Elsevier B.V. All rights reserved.
doi:10.1016/j.nimb.2007.03.076

form, fitted to *ab initio* values of both point defects and bulk properties [6]. The DD is also a many-body potential, but includes the effects of magnetism on the interaction energy between the atoms by using the Stoner and Ginzberg–Landau models [7]. MEA, on the other hand, is an angular dependent analytic bond-order potential fitted to *ab initio* as well as experimental values of cohesive energies, bond lengths and elastic constants of several structures with different coordination. It is able to reproduce the transition from alpha to gamma to delta phase of Fe. A comparison of the defect production predicted by these three different potentials, gives a good view of how sensitive the defect production properties are to modern potentials of comparable quality.

In MD simulations of collision cascades, it is important to have a realistic description of both the equilibrium material properties and the short-range behavior between recoiling nuclei. The original repulsive potential fit of the DD potential gives clearly too high threshold displacement energies (see below) and no repulsive potential fit was carried out during the construction of the MEA potential. Hence in the current paper we first adjust the repulsive parts of the DD and MEA potentials to obtain a good description of the threshold displacement energies. We call the modified potentials DD-BN and MEA-BN following recent naming practice [2]. The short ranged part of the AMS potential was not modified.

After the modifications, we compared the damage production predicted by the AMS, DD-BN and MEA-BN potentials by self-recoils in the energy range 0.5–20 keV.

The paper is organized as follows. First, we describe the procedure of the repulsive potential modifications. A description of the simulation and analysis methods is also given in the same section. The next section includes results and discussion. The potential modification results are presented and discussed in the first part of the section and the second part comprises of the recoil collision cascade results and a discussion thereof. Finally, the paper is concluded.

2. Method

2.1. Repulsive potential fit

During the initial stage of a recoil collision cascade, the movement of the atoms are governed by simple ballistic collisions with other atoms, and the interaction ranges in this phase are short. At these distances the forces between the atoms are purely repulsive, hence the evolution of a cascade depends on the repulsive part of the interatomic potential used. Moreover, this part of the potential also determines the formation and energetics of interstitial defects. A potential used in simulations of cascades is thus required to correctly describe the interaction taking place not only in the near-equilibrium range, but also at short distances.

A repulsive part is often added to a potential after having ensured that the equilibrium properties are described satisfactorily. A smooth join is preferable, but the process is complicated by the fact that very few well-defined experimental data to fit to exist. A purely *ad hoc* fitting, or the use of only one single observed property in the fitting, is frequent [6,10–14]. However, when fitting to the threshold displacement energies, one has to consider the fact that the threshold really is a 3D surface, hence the use of only a minimum value is inadequate. Moreover, one must also consider the melting temperature and the interstitial formation energies, which might be modified by the adjustment.

Available data, that were used for adjusting the repulsive part of the DD and the MEA potentials, are experimentally obtained thresholds [15,16] and defects formation energies calculated with DFT methods [17]. Both the AMS and the DD reproduce the interstitial energies well, but the DD predicts far too high threshold energies (see Section 3.1). The MEA, on the other hand, did not include any repulsive part. Therefore, by considering the above mentioned data, the DD and the MEA potentials were given adjusted repulsive parts. The resulting fits are, however, compromises, since it was impossible to completely separate the regions that affected only the threshold energies from those affecting the interstitials. The effect on the melting properties, cohesion energy and vacancy formation energy was also checked.

The pair function $V_{\mathrm{DD}}(r)$ of the DD was modified by letting the interactions at short distances be dictated by the universal screened Coulomb potential $V_{\mathrm{ZBL}}(r)$ [18], modified only by subtracting a constant V_0 (and thus denoted with an $*$), and a merging interpolation function $V_{\mathrm{int}}(r)$. The electronic structure calculations on which the ZBL potential is based are optimized only for high-energy interactions and are not meaningful at energies of a few eV [18], hence introducing a small constant shift in the ZBL potential as a fitting parameter can be done without altering the physically meaningful part of the potential. Note, moreover, that the atom dynamics is only governed by the forces $\mathrm{d}V/\mathrm{d}r$ between atoms, and hence the introduction of the constant does not change the atom trajectories in high-energy collisions.

The density function of the modified potential, DD-BN, is the original one, and the pair function is of the following form:

$$V_{\text{DD-BN}}(r) = V^{*}_{\mathrm{ZBL}}(r), \quad r \leqslant r_1 \tag{1}$$

$$= V_{\mathrm{int}}(r), \quad r_1 < r < r_2 \tag{2}$$

$$= V_{\mathrm{DD}}(r), \quad r \geqslant r_2, \tag{3}$$

where r_1 and r_2 equals 1.50098 and 2.25044 Å, respectively. The rather large interval was required to get a smooth interpolation. $V_{\mathrm{DD}}(r)$ is Eq. (43) in [7] and $V_{\mathrm{int}}(r)$ is a fifth-order polynomial,

$$V_{\mathrm{int}}(r) = a_0 + a_1 r + a_2 r^2 + a_3 r^3 + a_4 r^4 + a_5 r^5, \tag{4}$$

which was constructed to give a continuous potential and first and second derivatives at r_1 and r_2. The fitting was

done manually. Table 1 shows the resulting polynomial constants.

A different approach was used in the modification of the MEA. As done previously for Tersoff-like many-body potentials [12,13], a total potential V_{Tot} was constructed by joining the original universal ZBL repulsive potential $V_{\mathrm{ZBL}}(r)$ [18] with the equilibrium MEA potential $V_{\mathrm{Eq}}(r)$ using

$$V_{\mathrm{Tot}}(r) = V_{\mathrm{ZBL}}(r)(1 - F(r)) + V_{\mathrm{Eq}}(r)F(r), \tag{5}$$

where V_{Eq} is the potential for states close to equilibrium described in the main text of [9] and the Fermi function

$$F(r) = \frac{1}{1 + \mathrm{e}^{-b_{\mathrm{f}}(r - r_{\mathrm{f}})}}. \tag{6}$$

Note that the Fermi function is used here merely as a function which smoothly goes from 1 to 0 in a relatively narrow r interval, with no connection to the Fermi level of the electrons of the solid. The value of the constants b_{f} and r_{f} are chosen such that the potential is essentially unmodified at the equilibrium and longer bonding distances and that a smooth fit at short separations with no spurious minima is achieved for all realistic coordination numbers. As for the DD potential join, the joining constants were manually optimized to give a good description of the threshold displacement energies without affecting the interstitial energies overly much.

The threshold energies were calculated as in [19]. To summarize, recoil cascades initiated by recoils directed in angles in an interval of 0.2 Miller indices around the three principal directions, $\langle 1\,0\,0\rangle$, $\langle 1\,1\,0\rangle$ and $\langle 1\,1\,1\rangle$, as well as in random directions, were performed. In this way, both the direction specific thresholds $E_{\mathrm{d}}(\theta,\phi)$ and an average threshold $E^{\mathrm{av}}_{\mathrm{d,ave}}$ were obtained. The recoil energy was increased in steps of 2 eVs and possible defects in each run were identified using Wigner–Seitz (WS) cells [20] and by detecting an increase (of more than 4 eV) in the potential energy of the system. The average number of defects produced in the simulations was also obtained to be used in calculating the defect cross-section, a property comparable to experiments.

The melting temperature of iron as predicted by the different potentials was determined by simulating a solid–liquid interface at zero pressure and different temperatures [21]. The melting temperature was defined as the temperature at which the system was in equilibrium, i.e. when the fractions of solid and liquid parts remained constant. The simulations were performed for 50 ps.

Table 1
Polynomial coefficients of the interpolation function (Eq. (4)) used in the modification of the repulsive part of the DD-BN potential

n	a_n
0	$0.72470528950874 \times 10^3$
1	$-1.08800988724793 \times 10^3$
2	$0.48788202708644 \times 10^3$
3	$0.01143649654722 \times 10^3$
4	$-0.05832166589588 \times 10^3$
5	$0.01071895775243 \times 10^3$

Two features, describing a potential at short distances, have also been observed to correlate with the behavior of a cascade and the production of replacement collision sequences (RCS) [5,22]. These are the range R, defined as the interatomic distance at which the interaction energy equals 30 eV, and the stiffness S, which is the gradient calculated at that distance. These parameters are affected by the stiffening of a potential. A high ratio S/R describes a stiff potential and is proposed to lead to an increase in the number of RCSs, and thus also to produce larger and not very dense cascade volumes and shorter recombination times. A dense cascade and a long recombination time is attributed to a low S/R ratio [5,22]. We checked whether the same correlation is found in the cascades of potentials used in this work.

2.2. Cascade simulations and defect analysis

The recoil cascade simulation methods and defect analysis were the same as in [1]. The simulations were performed with the MD code PARCAS [23]. The simulation cells were at first relaxed for 10 ps at 0 kbar, 300 K after which a recoil near the center was given an energy ranging from 0.5 keV up to 20 keV in a random direction. Excess heat was removed from the two outermost atom layers and no recoiling atoms were allowed to hit the borders. The temperature was controlled with the Berendsen method [24]. A variable time step and periodic boundaries but no electronic stopping were used. Information about the number of cascades performed, the simulation time and the size of the simulation cells for each recoil energy and potential, is given in Table 2.

WS cells were employed to find the defects produced in the cascade simulations. An empty cell corresponded to a vacancy and multiply filled cells were defined as interstitials. A clustered fraction of the two defect types was also obtained. The cutoff radius in the cluster analysis was second nearest neighbor and third nearest neighbor for the vacancy and interstitial defects, respectively. These particular cutoffs correspond to those used in other studies, e.g. [1,5], thus simplifying comparisons.

Cells of 1025 and 1023 atoms were used in calculating the interstitial and vacancy formation energies, respectively. The simulations were performed at 0 K and the formation energy of a certain defect structure, $E^{\mathrm{f}}_{\mathrm{def}}$, was found using

$$E^{\mathrm{f}}_{\mathrm{def}} = E^{\mathrm{tot}}_{\mathrm{def}} - N \cdot E_{\mathrm{coh}}, \tag{7}$$

where $E^{\mathrm{tot}}_{\mathrm{def}}$ is the energy of the relaxed defect cell containing N atoms and E_{coh} is the cohesive energy of iron as predicted by the potential [25]. Long relaxation times and a small time step were employed.

Table 2
The number of cascades performed, the simulation time and the size of the simulation cell for each recoil energy and potential used in this work

Recoil energy (keV)	No. of events			Time (ps)	Box size (a_0)	No. of atoms
	AMS	MEA-BN	DD-BN			
0.5	20	20	20	25	20	16,000
1	20	20	20	25	25	31,250
2	20	20	20	25	31	59,582
5	100	40	20	25	42	148,176
10	15	20	15	25	54	314,928
20	25	15	15	25	67	601,526

3. Results and discussion

3.1. Results of the repulsive potential fit

In the construction of the DD-BN potential, the fitting procedure resulted in a value of $V_0 = 4.5$ eV for the ZBL offset and in coefficients of the interpolation polynomial (Eq. (4)) given in Table 1. With this polynomial, the DD-BN dimer interaction at short distances became of the form seen in Fig. 1(a). For the MEA-BN join the Fermi function constants $r_f = 0.95$ Å and $b_f = 2.90 \times 1/\text{Å}$ were obtained. The fit is illustrated in Fig. 1(b).

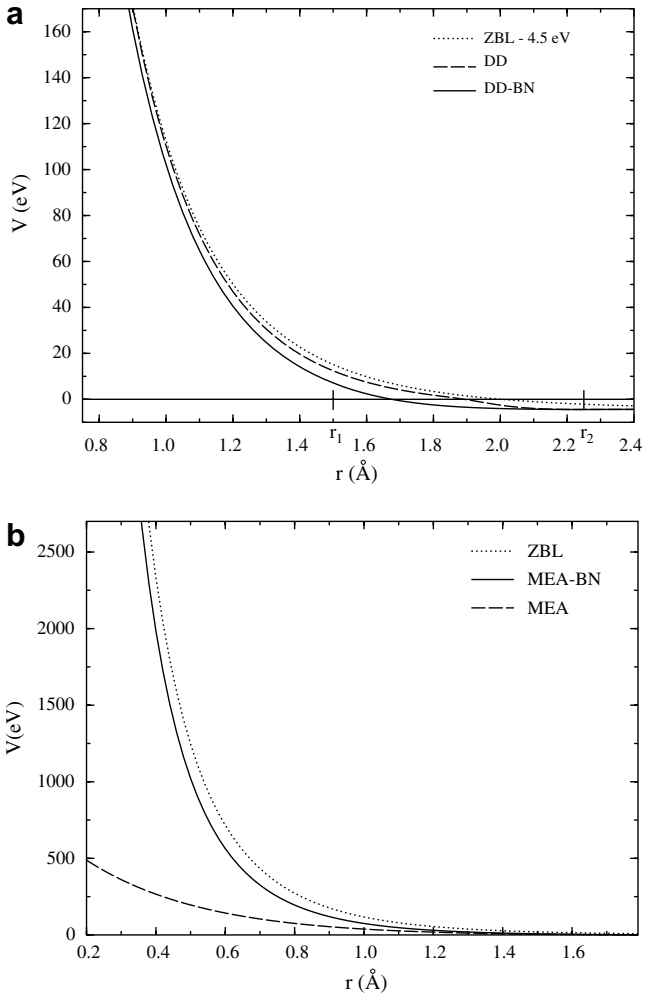

Fig. 1. The original DD and the modified DD-BN dimer interaction energy: (a) r_1 and r_2 indicates the interpolation range and ZBL is the universal screened Coulomb potential [18] and (b) illustrates the corresponding energy for the MEA and MEA-BN potentials.

The results of the threshold calculations for the DD-BN and the MEA-BN are shown in Table 3. Threshold energies in the principal directions as obtained from three experiments are included in the same table. The energies predicted by the modified potentials are in close agreement with the experimental values.

Excellent agreement is found when comparing the defect cross-section predicted by the potentials (see Fig. 2) with that of an experiment [26]. The calculation methods are described in [19]. Note that the experimental $\sigma(E)$ data is for each electron energy E an integral over atomic recoil energies T up to the maximum energy transfer T_m corresponding to the electron energy E [19]. Hence the $\sigma(E)$ data are dominated by the lowest threshold energies. This explains why the DD-BN and the MEA-BN data in the figure are very similar, even though their average thresholds differ.

The modifications of the potentials altered the interstitial formation energies slightly. The unmodified potential

Table 3
Threshold displacement energies in eV as predicted by the different potentials

Potential	$N_{\text{directions}}$	$E_d(\theta,\phi)$				$E^{av}_{d,ave}$
		All	⟨100⟩	⟨110⟩	⟨111⟩	
DD	2584	33	33	51	35	66.5 ± 0.5
DD-BN	2714	17	17	29	25	35.0 ± 0.4
MEA	2933	15	15	23	19	36.9 ± 0.3
MEA-BN	2591	17	17	25	23	42.3 ± 0.3
AMS	2699	16	17	33	33	40.0 ± 0.3
Exp.[a]		16–18				
Exp.[b]			17	>30	20	
Exp.[c]			20	30		

$N_{\text{directions}}$ is the number of directions that was used in determining the minimum $E_d(\theta,\phi)$ and the average threshold $E^{av}_{d,ave}$. The uncertainty of the values (except for the average threshold) is 1 eV, due to the energy step of 2 eV used in the calculations. The direction specific thresholds are calculated in an interval of 0.2 Miller index around the principal directions. Experimental values are also included.

[a] [26].
[b] [15].
[c] [16].

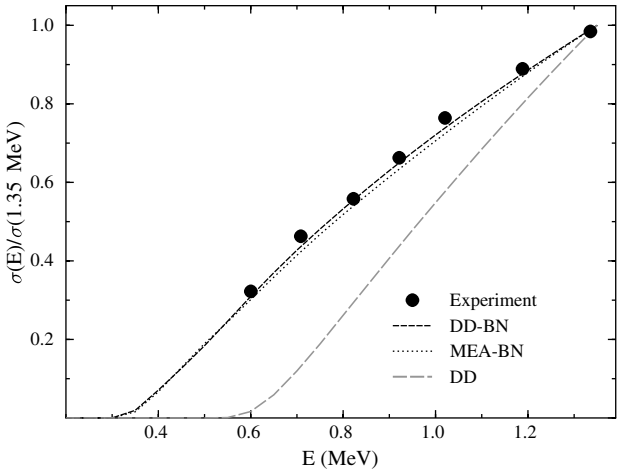

Fig. 2. The defect cross-section as a function of electron energy as predicted by the two modified potentials DD-BN and MEA-BN compared to experimental values [26]. The unmodified potential DD is also included to show the effect of the modification of the repulsive part.

DD predicted formation energies close to the *ab initio* values, whereas MEA gave higher values (see Table 4). After adjusting the repulsive parts, the DD-BN still predicts the ⟨1 1 0⟩ interstitial to be the most stable defect, with an energy difference of 0.43 eV and 0.74 eV to the ⟨1 1 1⟩ and ⟨1 0 0⟩ interstitial, respectively. The absolute values are, however, slightly lower than according to *ab initio* calculations. A correct order of the defects is found in the MEA-BN as well, although the fit resulted in an energy increase. The fit did not affect the vacancy formation of either potential but had a small affect of ~2% on the cohesive energy in the MEA-BN potential. It is vital to have a correct description of the interstitial energetics when modeling cascade damage, since it affects the mobility of interstitials and interstitial clusters [27] and thus also the clustered fractions.

The defect energetics of the AMS, the calculated melting temperature, as well as the range and the stiffness of the potentials, are also included in Table 4. The AMS is the only potential that predicts a melting temperature close to the experimental value, whereas temperatures as high as about 2300 K are required for melting in the MEA-BN. A large overestimation of the temperature is also seen in the DD-BN. A different description of the melting point affects the life time of the melted cascade core and the movement of vacancies towards the center [28]. Differences between cascades ascribable to this is indeed observed (see Section 3.2). Considering the range and stiffness of the potentials, the MEA-BN is the most stiff one, i.e. has the smallest range and a highest S/R ratio. The other two potentials are similar in stiffness.

3.2. Collision cascade results

The number of Frenkel pairs (FP) after the recoil collision cascades is shown in Fig. 3. The shaded area included in the figure represents the distribution of the number as predicted by earlier iron potentials. The data are taken from a recent review [2, and references therein]. The fluctuations between the potentials used in this work are seen to be small. This supports the notion that the threshold energies predicted by the potentials have a limited influence on the surviving defects in a cascade simulation [2,5].

Fig. 4 illustrates the evolution of the average number of FPs with time in 10 keV cascades. The AMS is seen to predict the largest number of defects at peak-time (when the maximum amount of defects are produced), but the number is the same as predicted by the other potentials after the recombination phase. The MEA-BN shows a shorter peak-time (500 fs as compared to 750 fs for the AMS and the DD-BN), a shorter relaxation time and only half as much FPs at peak-time as the other two. The largest difference is seen after the end of the ballistic phase, at about 1 ps. Correlation is thus found between the stiffness of a potential and the cascade behavior, since the stiffest potential, in this case the MEA-BN, predicts the least amount of

Table 4
Defect formation energies E^f_{def}, cohesion energy E_{coh}, melting temperature T_{melt}, range R and stiffness S of the original and modified potentials

	Ab initio[a]	Exp.	DD	DD-BN	MEA	MEA-BN	AMS
E^f_{vac} (eV)	2.07	1.5–2.2 eV[b]	1.97	1.97	1.56	1.56	1.71
$E^f_{\langle 100\rangle}$ (eV)	4.64		4.61	4.22	5.50	5.78	4.45
$E^f_{\langle 111\rangle}$ (eV)	4.34		4.28	3.91	4.51	4.75	4.12
$E^f_{\langle 110\rangle}$ (eV)	3.64	Stable, 4.7–5.0[c]	3.67	3.48	4.17	4.52	3.67
E_{coh} (eV)		−4.32[d]	−4.316	−4.316	−4.280	−4.178	−4.013
T_{melt} (K)		1811[e]	2175 ± 25	2125 ± 25	2225 ± 25	2300 ± 25	1750 ± 25
R (Å)			1.38	1.33	0.87	1.05	1.33
S (eV/Å)			−101	−119	−102	−140	−130
$\lvert S/R\rvert$ (eV/Å^2)			73	89	118	134	98

Available *ab initio* and experimental data are also given.
[a] [17].
[b] [29–33].
[c] [34].
[d] [35].
[e] [33].

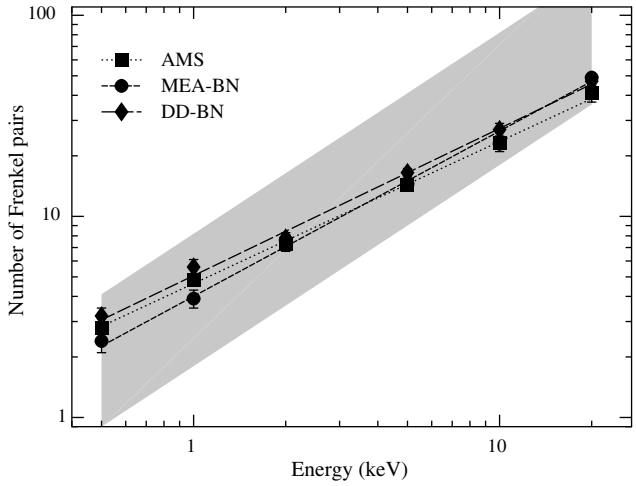

Fig. 3. The number of Frenkel pairs produced in cascade simulations. The shaded area shows the distribution of the amount as predicted by earlier potentials.

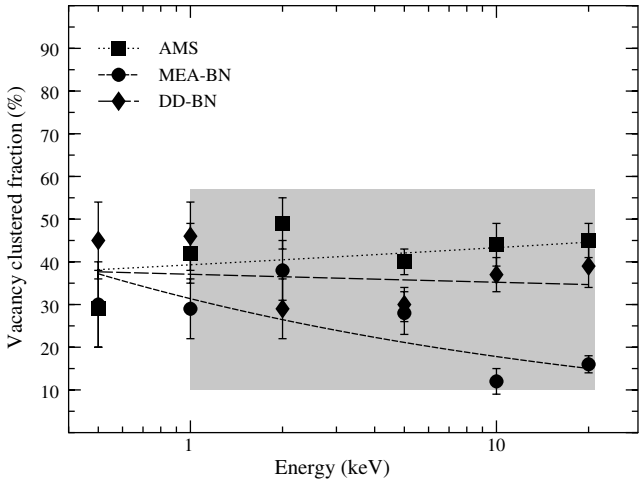

Fig. 5. Vacancy clustered fraction as a function of recoil energy. The shaded area represents the distribution of the fraction as predicted by earlier iron potentials.

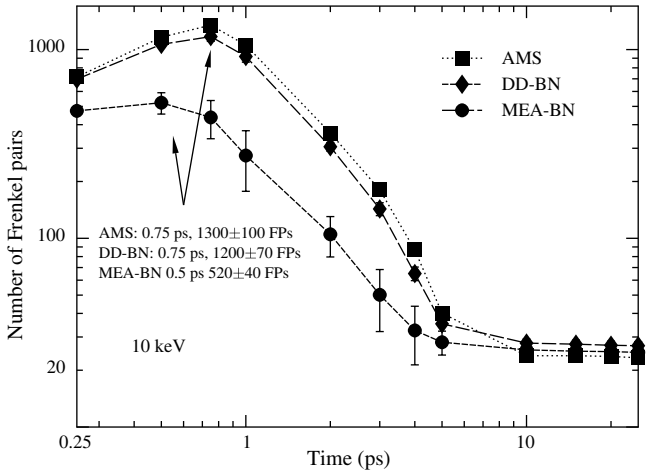

Fig. 4. The average number of Frenkel pairs as a function of time in collision cascades initiated by 10 keV recoils.

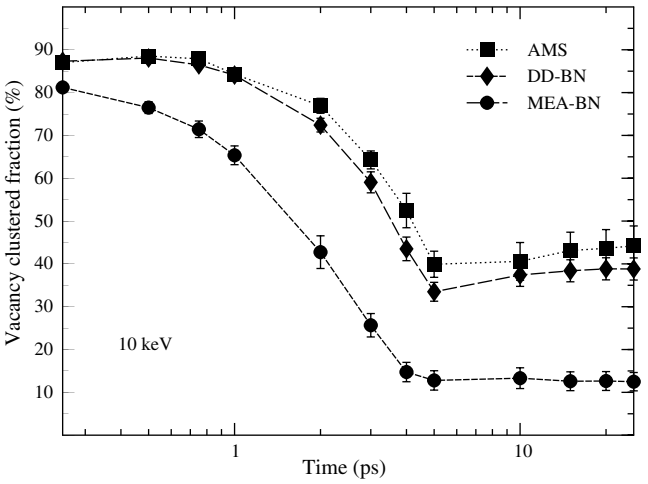

Fig. 6. The vacancy clustered fraction as a function of time in 10 keV cascades.

damage at peak-time. Denser cascades and more defects are observed in the softer potentials AMS and DD-BN. Noteworthy is, however, the close agreement on the amount at the end of the cascades.

A comparison between the clustered fractions predicted by the potentials does not show the same agreement (Figs. 5 and 7). The fraction of vacancies in clusters within the MEA-BN is at high recoil energies lower, at values $\lesssim$15%, than the ones in the other two potentials. At lower energies, the fraction is roughly between 30% and 50% for all potentials. The highest fraction is achieved using the AMS.

When studying the vacancy fraction of the 10 keV cases a bit closer, that is, looking at how the vacancy fraction evolves during the cascades, one notices that the lower fraction predicted by the MEA-BN is achieved rather fast (see Fig. 6). The same behavior is seen also in 5 keV cascades. The fraction within this potential is decreasing even after the thermal spike, in contrast to the DD-BN and the AMS, where the fractions are exhibiting a slight increase during the same time. The vacancy clustered fraction has been proposed to be related to the melting point of a material, since the lattice recrystallization front pushes the vacancies towards the center of the cascade [36,37]. A higher melting point leads to a faster movement of the recrystallization front inwards. This leaves less time for vacancies to migrate towards the center and instead makes them more likely to freeze in the lattice further away. Hence a high melting point can be expected to correlate with less vacancy clustering. One can indeed see that the potential having the highest melting point (MEA-BN) results in the lowest fraction and the one having the lowest melting point (AMS) in the highest fraction. At low recoil energies no heat spike liquid zone exists and thus no recrys-

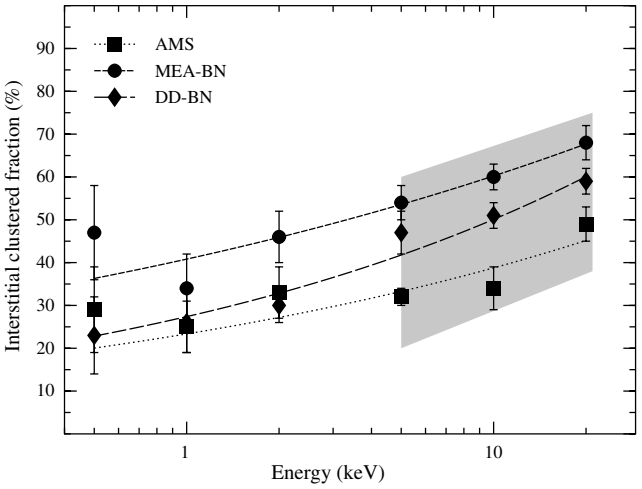

Fig. 7. Interstitial clustered fraction as a function of recoil energy. The fractions were calculated using a cluster connectivity cutoff corresponding to the third nearest neighbor.

tallization front. Hence the difference is only visible at the higher energies.

All the potentials predict similar behavior of the interstitial clustered fraction (Fig. 7), since all the fractions are seen to increase with energy. The MEA-BN predicts in this case the largest fraction of the three potentials and the AMS the smallest. The values lie, however, in the interval of fractions predicted by earlier potentials (illustrated by the shaded area in the figure). Two features of the AMS, namely the low fraction of interstitials in clusters and the tendency to produce about the same fraction of vacancy and interstitial clusters, have also previously been observed [5].

Fig. 8 shows the behavior of the interstitials clustered fraction with time. Two things can be pointed out: the increase of the fraction at the recombination phase, which only the MEA-BN and the DD-BN show, and the small

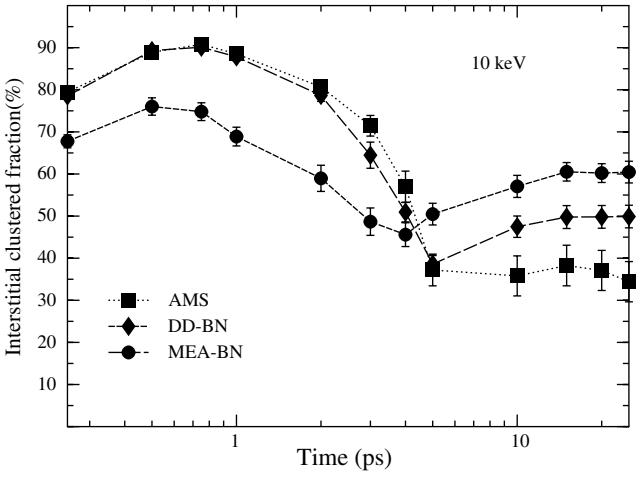

Fig. 8. The fraction of interstitials in clusters as a function of time in 10 keV cascades.

drop from maximum to minimum of the MEA-BN. This could be explained by the mobility of the interstitials. The interstitial migration energy E_{mig} in the AMS is relatively high, about 0.25–0.3 eV [38], hence the thermally induced interstitial mobility is expected to be lower than in the DD-BN and the MEA-BN, where the migration energies are smaller. The values are within the original potentials $E_{\mathrm{mig}}^{\mathrm{DD}} = 0.15$ eV and $E_{\mathrm{mig}}^{\mathrm{MEA}} = 0.17$ eV [9], respectively. (We checked whether the modifications of the repulsive parts altered these values, noticing only a minor effect of $\lesssim 0.02$ eV.) The difference in mobility is visible in the fact that the interstitial clustering fraction remains constant during the end of the cascades within the AMS, while the interstitials are able to rearrange and form clusters in the other potentials.

These results suggest that in order to obtain a quantitative description of the defect clustering, a potential must be able to correctly reproduce both the formation and the migration energies of defects. In this sense, the AMS can be considered as the most reliable of the three potentials studied in this work, since it predicts defect energies closest to *ab initio* values.

4. Conclusions

Molecular dynamic simulations of recoil collision cascades in Fe were performed with three recent potentials, including a magnetic many-body potential (DD), an analytic bond-order potential (MEA) and a many-body potential (AMS) previously studied. The potentials have different physical basis and different functional forms, but all reproduce the interstitial energetics well. The DD and the MEA were given realistic repulsive parts by adjusting them to reproduce experimentally obtained threshold energies and thus renamed DD-BN and MEA-BN, respectively.

The defect analysis revealed overall agreement between the potentials when it comes to the number of surviving defects after the cascade, but show that the defect clustered fraction still has some variation. A comparison with the fractions predicted by previous potentials does, however, show that the fluctuations are smaller. The differences between the fractions are ascribed to the different descriptions of the melting point and of the interstitial mobility in the potentials.

Acknowledgements

This work, supported by the European Communities under the contract of Association between EURATOM/Tekes, was carried out within the framework of the European Fusion Development Agreement. The views and opinions expressed herein do not necessarily reflect those of the European Commission. The research was performed within the Finnish Centre of Excellence in Computational Molecular Science (CMS), financed by The Academy of Finland and the University of Helsinki.

References

[1] C. Björkas, K. Nordlund, L. Malerba, D. Terentyev, P. Olsson, J. Nucl. Mater., accepted for publication.
[2] L. Malerba, J. Nucl. Mater. 351 (2006) 28.
[3] D.J. Bacon, T. Diaz de la Rubia, J. Nucl. Mater. 216 (1994) 275.
[4] R.S. Averback, T. Diaz de la Rubia, Displacement damage in irradiated metals and semiconductors, in: H. Ehrenfest, F. Spaepen (Eds.), Solid State Physics, Vol. 51, Academic Press, New York, 1998, p. 281.
[5] D. Terentyev, C. Lagerstedt, P. Olsson, K. Nordlund, J. Wallenius, L. Malerba, J. Nucl. Mater. 351 (2006) 65.
[6] G.J. Ackland, M.I. Mendelev, D.J. Srolovitz, S. Han, A.V. Barashev, J. Phys.: Condens. Matter 16 (2004) S2629.
[7] S.L. Dudarev, P.M. Derlet, J. Phys.: Condens. Matter 17 (2005) 1.
[8] J. Tersoff, Phys. Rev. B 37 (1988) 6991.
[9] M. Müller, P. Erhart, K. Albe, Phys. Rev. B, submitted for publication.
[10] N. Soneda, T. Diaz de la Rubia, Philos. Mag. A 78 (1998) 995.
[11] K. Albe, K. Nordlund, J. Nord, A. Kuronen, Phys. Rev. B 66 (2002) 035205.
[12] K. Albe, K. Nordlund, R.S. Averback, Phys. Rev. B 65 (2002) 195124.
[13] K. Nordlund, J. Keinonen, T. Mattila, Phys. Rev. Lett. 77 (1996) 699.
[14] M.I. Mendelev, S. Han, D.J. Srolovitz, G.J. Ackland, D.Y. Sun, M. Asta, Philos. Mag. 83 (2003) 3977.
[15] F. Maury, M. Biget, P. Vajda, A. Lucasson, P. Lucasson, Phys. Rev. B 14 (1976) 5303.
[16] J.N. Lomer, M. Pepper, Philos. Mag. 16 (1967) 119.
[17] C.-C. Fu, F. Willaime, P. Ordejón, Phys. Rev. Lett. 92 (2004) 175503.
[18] J.F. Ziegler, J.P. Biersack, U. Littmark, The Stopping and Range of Ions in Matter, Pergamon, New York, 1985.
[19] K. Nordlund, J. Wallenius, L. Malerba, Nucl. Instr. and Meth. B 246 (2006) 322.
[20] See e.g. N.W. Ashcroft, N.D. Mermin, Solid State Physics, Saunders, Philadelphia, 1976 (Section 4).
[21] J.R. Morris, C.Z. Wang, K.M. Ho, C.T. Chan, Phys. Rev. B 49 (1994) 3109.
[22] C.S. Becquart, A. Souidi, M. Hou, Phys. Rev. B 66 (2002) 134104.
[23] K. Nordlund, M. Ghaly, R.S. Averback, M. Caturla, T. Diaz de la Rubia, J. Tarus, Phys. Rev. B 57 (1998) 7556.
[24] H.J.C. Berendsen, J.P.M. Postma, W.F. van Gunsteren, A. DiNola, J.R. Haak, J. Chem. Phys. 81 (1984) 3684.
[25] G.-X. Qian, R.M. Martin, D.J. Chadi, Phys. Rev. B 38 (1988) 7649.
[26] P.G. Lucasson, R.M. Walker, Phys. Rev. 127 (1962) 485.
[27] Y.N. Osetsky, D.J. Bacon, A. Serra, B.N. Singh, S.I. Golubov, J. Nucl. Mater. 276 (2000) 65.
[28] K. Nordlund, L. Wei, Y. Zhong, R.S. Averback, Phys. Rev. B 57 (1998) 13965.
[29] L. De Schepper, D. Segers, L. Dorikens-Vanpraet, M. Dorikens, G. Knuyt, L. Stals, P. Moser, Phys. Rev. B 27 (9) (1983) 5257.
[30] K. Maier, H. Metz, D. Herlach, H.-E. Schaefer, J. Nucl. Mater. 69–70 (1978) 589.
[31] H. Matter, J. Winter, W. Triftháuser, Appl. Phys. 20 (1979) 135.
[32] A. Seeger, Phys. Status Solidi A 167 (1998) 289.
[33] P. Ehrhart, Properties and interactions of atomic defects in metals and alloys, Landolt-Börnstein, New Series III, Vol. 25, Springer, Berlin, 1991, p. 88 (Chapter 2).
[34] H. Wollenberg, Physical Metallurgy, Vol. 2, North-Holland, 1996.
[35] D.R. Lide, CRC Handbook of Chemistry and Physics, 82nd ed., CRC Press, LLC, Boca Raton, FL, USA, 2001.
[36] K. Nordlund, M. Ghaly, R.S. Averback, J. Appl. Phys. 83 (1998) 1238.
[37] K. Nordlund, R.S. Averback, Phys. Rev. B 59 (1999) 20.
[38] F. Willaime, C. Fu, M. Marinica, J.D. Torre, Nucl. Instr. and Meth. B 228 (2005) 92.